Applied Physics Letters

Quality factor tuning of micromechanical resonators via electrical dissipation

Cite as: Appl. Phys. Lett. **116**, 023506 (2020); https://doi.org/10.1063/1.5125286
Submitted: 22 August 2019 . Accepted: 26 December 2019 . Published Online: 16 January 2020

Nicholas E. Bousse, James M. L. Miller, Hyun-Keun Kwon, Gabrielle D. Vukasin, and Thomas W. Kenny

ARTICLES YOU MAY BE INTERESTED IN

Oxygen octahedral tilt ordering in $(Na_{1/2}Bi_{1/2})TiO_3$ ferroelectric thin films
Applied Physics Letters **116**, 022902 (2020); https://doi.org/10.1063/1.5127212

Interplay between emission wavelength and s-p splitting in MOCVD-grown InGaAs/GaAs quantum dots emitting above 1.3 μm
Applied Physics Letters **116**, 023102 (2020); https://doi.org/10.1063/1.5124812

Existence and stability of skyrmion bags in thin magnetic films
Applied Physics Letters **116**, 022413 (2020); https://doi.org/10.1063/1.5127173

© 2020 Author(s).

Applied Physics Letters ARTICLE scitation.org/journal/apl

Quality factor tuning of micromechanical resonators via electrical dissipation

Cite as: Appl. Phys. Lett. **116**, 023506 (2020); doi: 10.1063/1.5125286
Submitted: 22 August 2019 · Accepted: 26 December 2019 ·
Published Online: 16 January 2020

Nicholas E. Bousse,[a] James M. L. Miller,[b] Hyun-Keun Kwon, Gabrielle D. Vukasin, and Thomas W. Kenny

AFFILIATIONS

Departments of Mechanical and Electrical Engineering, Stanford University, Stanford, California 94305, USA

[a]Electronic mail: nbousse@stanford.edu
[b]Electronic mail: jmlm@stanford.edu

ABSTRACT

Sensitive capacitive transduction of micromechanical resonators can contribute significant electrical dissipation, which degrades the quality factor of the eigenmodes. We theoretically and experimentally demonstrate a scheme for isolating the electrical damping of a mechanical resonator due to Ohmic dissipation in the readout amplifier. The quality factor suppression arising from the amplifier is strongly dependent on the amplifier feedback resistance and parasitic capacitance. By studying the thermomechanical displacement noise spectrum of a doubly clamped micromechanical beam, we confirm that electrical dissipation tunes the actual, not effective, quality factor. Electrical dissipation is an important consideration in the design of sensitive capacitive displacement transducers, which are a key component in resonant sensors and oscillators.

© *2020 Author(s). All article content, except where otherwise noted, is licensed under a Creative Commons Attribution (CC BY) license (http://creativecommons.org/licenses/by/4.0/).* https://doi.org/10.1063/1.5125286

Micro- and nanoelectromechanical (M/NEM) resonators are widely used as timing references,[1] inertial sensors,[2,3] and mass sensors.[4,5] The quality factor, Q, is the inverse measure of dissipation in M/NEM resonators and is one of their most important properties. Increasing Q improves the thermomechanical signal-to-noise ratio (SNR) in resonant sensors and reduces the phase noise in oscillators. Large Q also maximizes the effective cooling attainable with feedback or parametric coupling, which eases the temperature requirements for cooling the mode into its quantum ground state.[6–9] The quality factor is traditionally limited by mechanical losses, such as anchor damping,[10–12] thermoelastic dissipation (TED),[13,14] the Akhiezer effect,[15–17] and surface losses,[18,19] and so a great deal of work has gone toward understanding and minimizing these sources.

Dissipation may also arise from the electrostatic or magnetic coupling of the resonator to its external environment.[20–27] Electrical damping is distinct from the "effective" quality factor tuning mechanisms, which also often arise from electrical interactions, because electrical damping increases both the dissipation and the corresponding thermomechanical noise force.[28] For capacitive or magnetomotive detection, the resonator induces charge flow, which through Joule heating is dissipated in the resonator body, the measurement circuit, or in nearby grounded electrodes, increasing the linewidth. The associated Johnson noise acts back on the mechanical motion via the same electrical coupling path, increasing the thermomechanical noise force. Electrical damping is pronounced in electromechanical resonators constructed from carbon nanotubes, nanowires, and graphene because of the strong charge coupling and tiny inertia.[23,24,29–34] It also arises in nanomechanical resonators due to currents in the detection circuit,[20,21,35–37] Ohmic losses in the adjacent electrodes,[22,23,38–40] or dielectric losses in the body.[25,26,41]

In capacitively transduced micromechanical resonators, electrical damping is typically small compared to gas damping, anchor loss, thermoelastic dissipation, and other mechanical sources. The influence of the capacitive coupling of the MEM resonator to its external environment on the dissipation can often be ignored in this case. However, efforts to maximize SNR in MEM resonant sensors and oscillators can potentially lead to significant electrical damping in the resonator and detection circuit, to the point where the contribution from the intrinsic sources becomes negligible.

In this Letter, we study strongly electrically damped micromechanical resonators in a wafer-scale encapsulation process.[42] The maximized detection SNR achieved with micrometer capacitive gaps, a large electrode area, and a large transimpedance gain introduces significant electrical dissipation, which can ultimately dwarf the damping originating from mechanical sources. Our setup allows us to adjust the electrical damping arising from an adjacent capacitively coupled resistor to ground, the electrical loading by the amplifier, and the modification of Q arising from the dependence of resonant frequency on bias

© Author(s) 2020

voltage. This allows us to isolate the contribution of electrical damping in the amplifier to the total resonator dissipation. We propose a model for electrical losses in our capacitively transduced micromechanical resonator, analogous to the electrical damping models introduced for other M/NEM systems,[20,21,23–25,38] and validate it with experiments on a fabricated doubly clamped beam. By fitting the results from the fluctuation-dissipation theorem to the thermomechanical displacement noise spectrum in the presence of increasing electrical damping, we confirm that these dissipation sources correspond to an actual, not effective, change in the quality factor.

Figure 1 depicts the equivalent system for the doubly clamped beam resonator and measurement setup. Electrical contacts to the resonator and adjacent electrodes allow for capacitive sensing and electrical loading of the resonator. We capacitively monitor the thermomechanical motion with a low-noise transimpedance amplifier (TIA), which enables us to extract the quality factor, resonant frequency, and electromechanical transduction factor.[43] The beam is fabricated from single crystal silicon and is oriented in the [110] direction. It has a length of 600 μm, a width of 6 μm, and a device layer thickness of 60 μm. The capacitive gap size is roughly 1 μm. The lumped mass of the fundamental flexural mode is 82.73 ng.[43]

The circuit diagram for the TIA is depicted in Fig. 2 and consists of a transimpedance stage with a low-pass filter and an inverting amplifier stage with a bandpass filter. A third unity-gain buffer stage is used to maintain amplifier stability. Table I gives component values for the circuit. The influence of the first stage feedback resistor of the amplifier circuit, R_{f1}, on the electrical damping can be represented by an effective passive load,

$$R_E = \frac{R_{f1}}{1 + G_{OL}}, \tag{1}$$

where G_{OL} is the open-loop gain of the operational amplifier in the first inverting amplifier stage of the TIA.

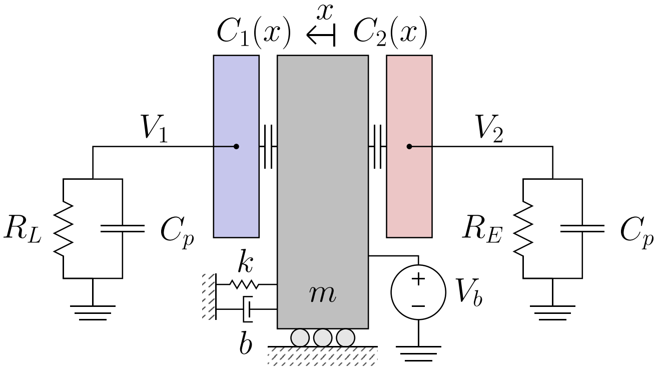

FIG. 1. The equivalent system for modeling electrical damping due to two coupled loads. The mass, m, is constrained to translate in the x direction and is connected to a spring, k, and dashpot, b. The mechanical system is coupled to two first-order electrical circuits via the position-dependent capacitances, $C_1(x)$ and $C_2(x)$. One circuit consists of a parasitic capacitance, C_p, and resistive load, R_L. The transimpedance amplifier (TIA) is attached to the opposing electrode to amplify the current resulting from the thermomechanical motion and is modeled as contributing a parasitic capacitance, C_p, and an equivalent load resistance, R_E.

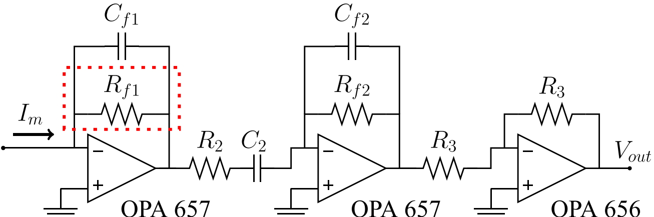

FIG. 2. A schematic of the transimpedance amplifier used to capacitively measure mechanical motion in our micromachined resonator. The three amplifiers used in Figs. 3 and 4 only differ in terms of the first stage feedback resistor, emphasized by the red dashed box in the schematic.

TABLE I. Transimpedance amplifier component values.

R_{f1}	C_{f1}	R_2	C_2	R_{f2}	C_{f2}	R_3
1–10 MΩ	0.01 pF	1 kΩ	10 nF	10 kΩ	10 pF	1 kΩ

By applying a bias voltage V_b between the beam and adjacent electrodes, the capacitive coupling will transduce the thermomechanical motion of the beam into a motional current out of the electrodes. Dissipation in the TIA connected to one electrode acts back on the motion as it amplifies the motional current into a voltage, lowering the Q value. Ohmic dissipation of the motional current in the electrical load resistor R_L connecting the opposing electrode to ground also contributes electrical damping. By systematically varying the load resistance and first stage amplifier feedback resistor, the electrical damping contributed by the load resistor and amplifier can be independently measured. We measure the amplitude spectral density (ASD) of the TIA output near resonance to extract the Q value as a function of V_b, R_L, and amplifier feedback resistor. No external drive forces are used, so the resonator remains in thermal equilibrium with its environment during the course of the measurements. The entire resonator and amplifier system is maintained at 30.0±0.1 °C using an electrically shielded, temperature controlled chamber. Chip-scale electrical connections to the resonator make a significant contribution to the parasitic capacitance, and so they were made once and left undisturbed throughout the duration of the experiments. To minimize the variation in the parasitic capacitance during the measurements, we make changes to the amplifier and load resistor via the external breakout board.

Figure 1 presents a second-order mechanical system coupled to two first-order electrical systems by two position-dependent capacitances, given by

$$C_1(x) = \frac{\gamma_c \epsilon_0 A}{g - x}, \quad C_2(x) = \frac{\gamma_c \epsilon_0 A}{g + x}, \tag{2}$$

where ϵ_0 is the permittivity of free space, A is the capacitor area, g is the gap size, and $\gamma_c = 0.52$ is the mode shape correction factor.[43] Applying the conservation of charge at the two electrodes leads to equations for the electrode voltages, which can be combined with the equation of motion for a simple harmonic oscillator to form a system of three coupled equations,

© Author(s) 2020

$$m_{eff}\,\ddot{x} + b\,\dot{x} + kx = F_e(x) + F_{th},$$
$$\frac{V_1}{R_L} + C_p\frac{dV_1}{dt} + \frac{d}{dt}\left[C_1(x)(V_1 - V_b)\right] = 0,$$
$$\frac{V_2}{R_E} + C_p\frac{dV_2}{dt} + \frac{d}{dt}\left[C_2(x)(V_2 - V_b)\right] = 0, \tag{3}$$

where V_b is the device bias voltage, F_e is the force from coupling to the electrical system, and F_{th} is the thermomechanical noise force. Using the Laplace transform, the equations for the electrical circuit can be expressed in the frequency domain,

$$V_1(x) = V_b j\omega(\alpha_1 - \beta_1 j)C_1(x),$$
$$V_2(x) = V_b j\omega(\alpha_2 - \beta_2 j)C_2(x). \tag{4}$$

Here, α and β are the parameters of the electrical circuit, which are given by

$$\alpha_1 = \frac{R_L}{1 + \omega^2 R_L^2 C_{t,1}^2}, \quad \beta_1 = \frac{\omega R_L^2 C_{t,1}}{1 + \omega^2 R_L^2 C_{t,1}^2},$$
$$\alpha_2 = \frac{R_E}{1 + \omega^2 R_E^2 C_{t,2}^2}, \quad \beta_2 = \frac{\omega R_E^2 C_{t,2}}{1 + \omega^2 R_E^2 C_{t,2}^2}, \tag{5}$$

where $C_{t,1} = C_p + C_1$ and $C_{t,2} = C_p + C_2$. Nominal device capacitance $C_{d,0} = C_1(x)|_{x=0}$ can be found using Eq. (2) to be 0.17 pF. Parasitic capacitance, which is dominated by the electrical contacts to the device through the encapsulation layer, is roughly 20 pF. Since the parasitic capacitance is several orders of magnitude larger than the capacitance across the gaps, C_t can be approximated as constant. As we show in the supplementary material, the relaxation time of the resonator is significantly larger than the relaxation time of the electrical circuit during these experiments, so the voltages V_1 and V_2 can be assumed to be uniform across the electrodes. These voltages lead to forces on the mechanical system via the coupling capacitances, which can be obtained with Coulomb's law,

$$F_e(x) = \frac{C_1^2(V_b - V_1)^2}{2\gamma_c A\epsilon_0} - \frac{C_2^2(V_b - V_2)^2}{2\gamma_c A\epsilon_0}. \tag{6}$$

Expanding Eq. (6) and keeping the terms at ω yield a force term that depends upon the position and velocity as

$$F_e = \left[2C_{d,0}^{-1} - \omega(\beta_1 + \beta_2)\right]\eta^2 x - (\alpha_1 + \alpha_2)\eta^2\,\dot{x}, \tag{7}$$

where $\eta = V_b \frac{\partial C_1}{\partial x}|_{x=0}$. Substituting Eq. (7) into Eq. (3) yields the governing equation for the mechanical system,

$$\ddot{x} + \frac{w_n}{Q}\dot{x} + \omega_n^2 x = \frac{F_{th}}{m_{eff}} \tag{8}$$

where Q is the quality factor and ω_n is the resonant frequency of the total system. The term proportional to x in Eq. (7) modifies the natural frequency of the resonator,

$$\omega_n = \sqrt{\frac{k}{m_{eff}} - \frac{2\eta^2}{m_{eff}C_{d,0}} + \frac{\omega_n(\beta_1 + \beta_2)\eta^2}{m_{eff}}}. \tag{9}$$

In this system, $\omega_n\beta$, which has a maximum value of $1/C_t$ for any value of R_e, is much smaller than $1/C_{d,0}$. Electrostatic softening in the device tunes the resonator natural frequency from $\omega_{n,0}/2\pi = 126$ kHz to as low as $\omega_n/2\pi = 84$ kHz across the 0–24 V bias voltage range used in Figs. 3 and 4. The term proportional to $\dot{x}$ in Eq. (7) modifies the quality factor of the mechanical system,

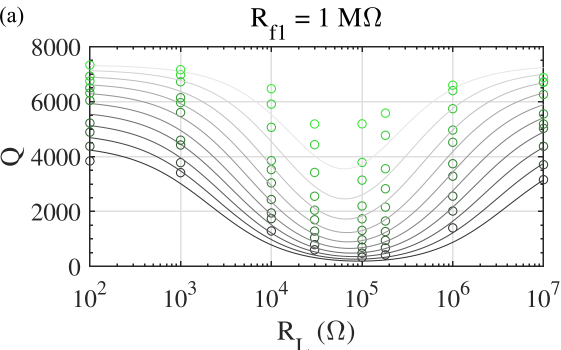

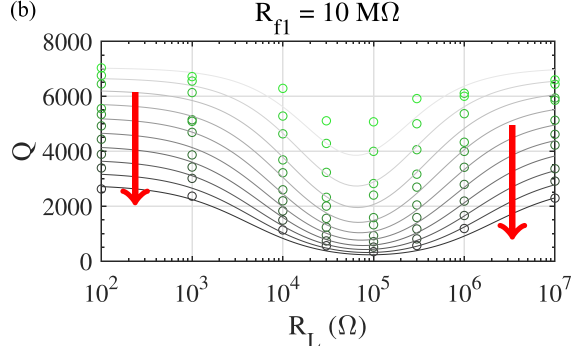

FIG. 3. The measured total quality factor, Q, as a function of the load resistor, R_L, and bias voltage, V_b, for (a) $R_{f1} = 1$ MΩ and (b) $R_{f1} = 10$ MΩ. V_b is varied from 6 V to 24 V in 2 V increments, with darker data points corresponding to higher voltages. The model in Eq. (11) is fitted using $C_t = 20$ pf and an effective amplifier resistance $R_E = 270$ Ω for $R_{f1} = 1$ MΩ and $R_E = 1.9$ kΩ for $R_{f1} = 10$ MΩ. The arrows indicate the reduction in Q for all R_L values, which accompanies the increased feedback resistance.

$$\frac{1}{Q} = \frac{b}{m_{eff}\omega_n} + \frac{\alpha_1\eta^2}{m_{eff}\omega_n} + \frac{\alpha_2\eta^2}{m_{eff}\omega_n}. \tag{10}$$

The quality factor can be written as a reciprocal sum,

$$\frac{1}{Q} = \frac{\omega_{n,0}}{Q_0\omega_n} + \frac{1}{Q_{e,1}} + \frac{1}{Q_{e,2}}, \tag{11}$$

where $Q_0 = m_{eff}\omega_{n,0}/b$ is the quality factor in the limit of zero bias voltage and $Q_{e,1}$ and $Q_{e,2}$ are the quality factors associated with the electrical coupling to a given electrode. For this device, Q_0 is dominated by thermoelastic dissipation (TED), in agreement with the Zener model.[44] Even in the absence of electrical damping, the significant electrostatic softening of the resonant frequency with increasing bias voltage reduces the quality factor. Substituting Eq. (5), evaluated at $\omega = \omega_n$, into the electrical quality factor terms in Eq. (10) yields

$$Q_{e,1} = \frac{m_{eff}\omega_n\left(\omega_n^2 C_{t,1}^2 R_L^2 + 1\right)}{\eta^2 R_L},$$
$$Q_{e,2} = \frac{m_{eff}\omega_n\left(\omega_n^2 C_{t,2}^2 R_E^2 + 1\right)}{\eta^2 R_E}. \tag{12}$$

© Author(s) 2020

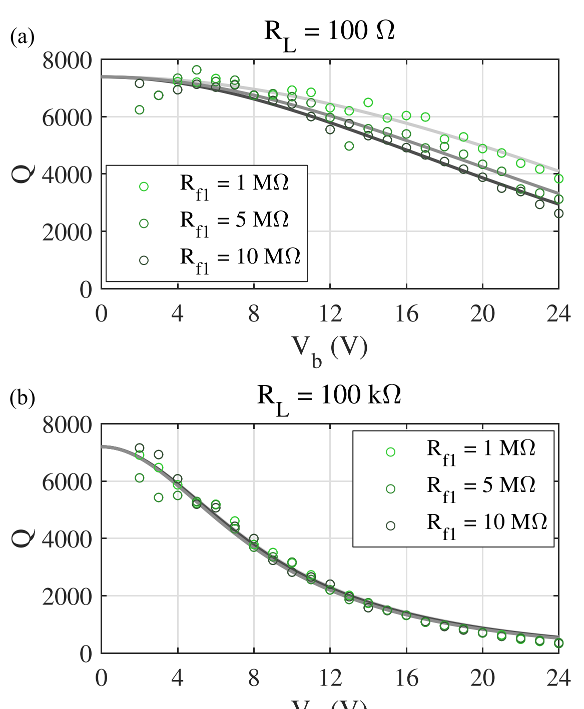

FIG. 4. The measured total quality factor, Q, as the bias voltage, V_b, is varied for three different amplifier configurations, (a) away from the cutoff frequency of the RC circuit for the load resistor $R_L = 100\ \Omega$ and (b) near the cutoff frequency of the RC circuit for $R_L = 100\,\mathrm{k\Omega}$.

The resonator motion due to its coupling to the thermal bath has a displacement noise ASD given by

$$X_{th}(\omega) = \frac{\sqrt{4k_B T b}}{m_{eff}\sqrt{\left(\omega_n^2 - \omega^2\right)^2 + \left(\frac{\omega\omega_n}{Q_{eff}}\right)^2}}, \tag{13}$$

where T is the temperature, k_B is Boltzmann's constant, and Q_{eff} is the effective quality factor of the resonator. $Q_{eff} = Q$ for our experiments, as all changes in the quality factor occur by modifying the underlying dissipation and the corresponding thermomechanical noise. As we show in the supplementary material, in the presence of electrical dissipation, the output voltage ASD near the resonance of a TIA connected to the electrode is given by

$$V_N(\omega) = \sqrt{\frac{\left(4k_B T G^2\right)\left(\frac{\eta^2}{m_{eff}}\right)\left(\frac{\omega^2\omega_n}{Q}\right)}{\left(\omega_n^2 - \omega^2\right)^2 + \left(\frac{\omega_n^2}{Q_{eff}}\right)^2} + N_a^2}, \tag{14}$$

where G is the transimpedance gain, η is the transduction factor,[45] N_a is the noise floor of the amplifier, and Q is the total quality factor given by Eq. (11). This equation presumes that the quality factor is sufficiently large that α_1 and α_2 are approximately constant near resonance.

Figure 3 plots the measured quality factor as a function of bias voltage and load resistance in the vicinity of the RC cutoff frequency. For all load resistor values, increasing the bias voltage strongly reduces Q, and Q reduction is maximum when the load resistor shifts the cutoff frequency of the RC circuit to match the mechanical resonance frequency.[24,38] We measure the voltage ASD near resonance and implement a least squares minimization fit to the model given by Eq. (14) to extract Q, η^2/m_{eff}, ω_n, and N_a. We present two different three-stage amplifiers, each one with a different first stage feedback resistor denoted by R_{f1}. We separately measure $G(\omega)$ for each TIA. We fit the quality factor as a function of R_L and V_b to the model in Eq. (11) by selecting the values for C_t, Q_0, and R_E. $C_t = 20$ pf and $Q_0 = 7530$ are used in all cases. No arbitrary scaling parameters are used. For $R_{f1} = 1\ \mathrm{M\Omega}$, the effective dissipation resistance is $R_E = 270\ \Omega$, while for $R_{f1} = 10\ \mathrm{M\Omega}$, the effective dissipation resistance is $R_E = 1.9\,\mathrm{k\Omega}$. The values extracted from the fitting are in agreement with the values expected from Eq. (1) for the open-loop gain values for an OPA657 amplifier: 65–70 dB.[46] The increased equivalent resistance in the amplifier corresponds to an increase in the effect of electrical damping away from the RC cutoff frequency, denoted by the arrows in Fig. 3.

Figure 4 demonstrates the impact of the measurement amplifier on the total quality factor, for a load resistance away from and near the cutoff frequency of the RC circuit. The Q suppression maximum seen at $R_L = 95\,\mathrm{k\Omega}$ in Fig. 3 corresponds to a cutoff frequency of $1/2\pi RC = 84$ kHz, which matches the resonant frequency of the device at $V_b = 24$ V. Away from the cutoff frequency, loss from the effective amplifier resistance, R_E, makes a non-negligible contribution to the total quality factor, so increasing R_{f1} results in an observable reduction in Q.

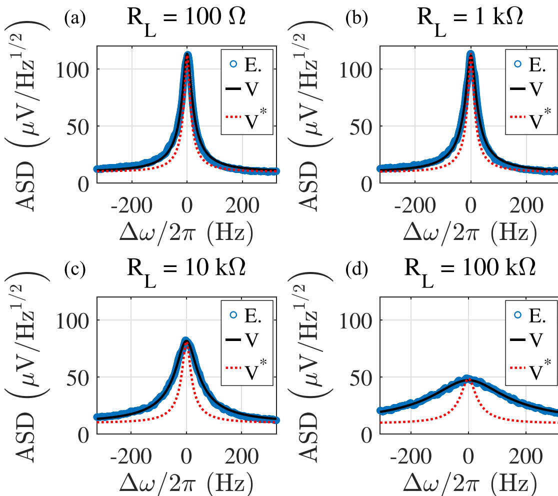

FIG. 5. (a)–(d) The amplitude spectral density (ASD) of the thermomechanical displacement noise as a function of the frequency offset from resonance, $\Delta\omega$, for the increasing load resistance, R_L. Experimental data are plotted against a least squares minimization fit, V, using Eq. (14), where $Q_{eff} = Q$, and, V^*, using Eq. (14), positing that electrical dissipation only decreases the effective quality factor, while the mechanical system quality factor remains in the limit of zero bias voltage. A close agreement of the $Q_{eff} = Q$ model with the experimental noise ASD suggests that electrical damping tunes the actual, not effective, quality factor of the resonator.

© Author(s) 2020

The electrical damping studied here differs from the methods of suppressing the effective quality factor because the Johnson noise in the resistance capacitively couples back to increase the thermomechanical noise force on the mechanical resonator.[47,48] Figure 5 demonstrates that the system matches the model in Eq. (14) when electrical damping is assumed to modify both the resonator transfer function and the thermomechanical noise force, i.e., both the numerator and denominator of Eq. (14), and does not match if the electrical damping is presumed to only modify the transfer function. Electrical damping thus reduces Q.

By sweeping the cutoff frequency of the secondary electrical circuit across the resonant frequency, we isolate the electrical damping of the mechanical resonator arising from the readout amplifier and show that the loss due to a high-gain amplifier can exceed the contributions from mechanical sources. We show that the electrical loss mechanism is strongly dependent on the parasitic capacitance within the system, suggesting that the geometry and fabrication method of electrodes for the capacitive sensing of resonators play important roles in determining the magnitude of electrical damping. We show that electrical damping suppresses the intrinsic quality factor, not the effective quality factor, of a M/NEM resonator.

See the supplementary material for the measurements of the electrical and mechanical relaxation times of the system and a derivation of the resonator noise ASD in the presence of electrical damping.

This work was supported by the National Science Foundation Collaborative Research Program under Grant No. 1662464. Fabrication was performed in nano@Stanford labs, which are supported by the National Science Foundation (NSF) as part of the National Nanotechnology Coordinated Infrastructure under Award No. ECCS-1542152, with support from the Defense Advanced Research Projects Agency's Precise Robust Inertial Guidance for Munitions (PRIGM) Program, managed by Ron Polcawich and Robert Lutwak.

REFERENCES

[1]See www.sitime.com, for "Sunnyvale, CA" (2019).
[2]R. Bogue, Sens. Rev. **27**, 7 (2007).
[3]D. D. Shin, C. H. Ahn, Y. Chen, D. L. Christensen, I. B. Flader, and T. W. Kenny, in *IEEE International Conference on Microelectromechanical Systems (MEMS)* (IEEE, 2017), pp. 17–20.
[4]W. Zhang and K. L. Turner, Sens. Actuators, A **122**, 23 (2005).
[5]V. Kumar, J. W. Boley, Y. Yang, H. Ekowaluyo, J. K. Miller, G. T.-C. Chiu, and J. F. Rhoads, Appl. Phys. Lett. **98**, 153510 (2011).
[6]D. Kleckner and D. Bouwmeester, Nature **444**, 75 (2006).
[7]J. D. Teufel, T. Donner, D. Li, J. W. Harlow, M. Allman, K. Cicak, A. J. Sirois, J. D. Whittaker, K. W. Lehnert, and R. W. Simmonds, Nature **475**, 359 (2011).
[8]J. Chan, T. P. M. Alegre, A. H. Safavi-Naeini, J. T. Hill, A. Krause, S. Gröblacher, M. Aspelmeyer, and O. Painter, Nature **478**, 89 (2011).
[9]D. J. Wilson, V. Sudhir, N. Piro, R. Schilling, A. Ghadimi, and T. J. Kippenberg, Nature **524**, 325 (2015).
[10]Y. Tsaturyan, A. Barg, E. S. Polzik, and A. Schliesser, Nat. Nanotechnol. **12**, 776 (2017).
[11]A. H. Ghadimi, S. A. Fedorov, N. J. Engelsen, M. J. Bereyhi, R. Schilling, D. J. Wilson, and T. J. Kippenberg, Science **360**, 764 (2018).
[12]J. Rodriguez, S. A. Chandorkar, G. M. Glaze, D. D. Gerrard, Y. Chen, D. B. Heinz, I. B. Flader, and T. W. Kenny, J. Microelectromech. Syst. **27**, 800 (2018).
[13]R. N. Candler, A. Duwel, M. Varghese, S. A. Chandorkar, M. A. Hopcroft, W.-T. Park, B. Kim, G. Yama, A. Partridge, M. Lutz, and T. W. Kenny, J. Microelectromech. Syst. **15**, 927 (2006).
[14]S. A. Chandorkar, R. N. Candler, A. Duwel, R. Melamud, M. Agarwal, K. E. Goodson, and T. W. Kenny, J. Appl. Phys. **105**, 043505 (2009).
[15]A. N. Cleland, *Foundations of Nanomechanics: From Solid-State Theory to Device Applications* (Springer, 2013).
[16]S. Ghaffari, S. A. Chandorkar, S. Wang, E. J. Ng, C. H. Ahn, V. Hong, Y. Yang, and T. W. Kenny, Sci. Rep. **3**, 3244 (2013).
[17]J. Rodriguez, S. A. Chandorkar, C. A. Watson, G. M. Glaze, C. H. Ahn, E. J. Ng, Y. Yang, and T. W. Kenny, Sci. Rep. **9**, 2244 (2019).
[18]D. W. Carr, S. Evoy, L. Sekaric, H. G. Craighead, and J. M. Parpia, Appl. Phys. Lett. **75**, 920 (1999).
[19]L. G. Villanueva and S. Schmid, Phys. Rev. Lett. **113**, 227201 (2014).
[20]A. N. Cleland and M. L. Roukes, Sens. Actuators, A **72**, 256 (1999).
[21]K. Schwab, Appl. Phys. Lett. **80**, 1276 (2002).
[22]I. Kozinsky, H. C. Postma, I. Bargatin, and M. Roukes, Appl. Phys. Lett. **88**, 253101 (2006).
[23]G. Jourdan, G. Torricelli, J. Chevrier, and F. Comin, Nanotechnology **18**, 475502 (2007).
[24]T. Barois, A. Ayari, A. Siria, S. Perisanu, P. Vincent, P. Poncharal, and S. Purcell, Phys. Rev. B **85**, 075407 (2012).
[25]J. Rieger, T. Faust, M. J. Seitner, J. P. Kotthaus, and E. M. Weig, Appl. Phys. Lett. **101**, 103110 (2012).
[26]J. Cha and C. Daraio, Nat. Nanotechnol. **13**, 1016 (2018).
[27]Y. Oikawa, H. Arisawa, S. Daimon, and E. Saitoh, Appl. Phys. Lett. **113**, 142407 (2018).
[28]J. M. L. Miller, A. Ansari, D. B. Heinz, Y. Chen, I. B. Flader, D. D. Shin, L. G. Villanueva, and T. W. Kenny, Appl. Phys. Rev. **5**, 041307 (2018).
[29]M. T. Woodside and P. L. McEuen, Science **296**, 1098 (2002).
[30]V. Sazonova, Y. Yaish, H. Üstünel, D. Roundy, T. A. Arias, and P. L. McEuen, Nature **431**, 284 (2004).
[31]J. S. Bunch, A. M. Van Der Zande, S. S. Verbridge, I. W. Frank, D. M. Tanenbaum, J. M. Parpia, H. G. Craighead, and P. L. McEuen, Science **315**, 490 (2007).
[32]A. Eriksson, S. Lee, A. A. Sourab, A. Isacsson, R. Kaunisto, J. M. Kinaret, and E. E. B. Campbell, Nano Lett. **8**, 1224 (2008).
[33]B. Lassagne, Y. Tarakanov, J. Kinaret, D. Garcia-Sanchez, and A. Bachtold, Science **325**, 1107 (2009).
[34]G. A. Steele, A. K. Hüttel, B. Witkamp, M. Poot, H. B. Meerwaldt, L. P. Kouwenhoven, and H. S. van der Zant, Science **325**, 1103 (2009).
[35]R. G. Knobel and A. N. Cleland, Nature **424**, 291 (2003).
[36]A. Naik, O. Buu, M. LaHaye, A. Armour, A. Clerk, M. Blencowe, and K. Schwab, Nature **443**, 193 (2006).
[37]P. A. Truitt, J. B. Hertzberg, C. Huang, K. L. Ekinci, and K. C. Schwab, Nano Lett. **7**, 120 (2007).
[38]Y. Deimerly, P. Rey, P. Robert, T. Bourouina, and G. Jourdan, in *IEEE International Conference on Microelectromechanical Systems (MEMS)* (IEEE, 2014), pp. 725–728.
[39]B. Fain, F. Souchon, A. Berthelot, R. Anciant, P. Robert, and G. Jourdan, in *IEEE International Conference on Inertial Sensors and Systems (INERTIAL)* (IEEE, 2018), pp. 1–4.
[40]B. Fain, F. Souchon, A. Berthelot, R. Anciant, P. Robert, and G. Jourdan, in *IEEE International Conference Microelectromechanical Systems (MEMS)* (IEEE, 2018), pp. 948–951.
[41]Q. P. Unterreithmeier, E. M. Weig, and J. P. Kotthaus, Nature **458**, 1001 (2009).
[42]Y. Yang, E. J. Ng, Y. Chen, I. B. Flader, and T. W. Kenny, J. Microelectromech. Syst. **25**, 489 (2016).
[43]J. M. L. Miller, N. E. Bousse, D. B. Heinz, H. J. Kim, H.-K. Kwon, G. D. Vukasin, and T. W. Kenny, J. Microelectromech. Syst. **28**(6), 965–976 (2019).
[44]C. Zener, Phys. Rev. **53**, 90 (1938).
[45]V. Kaajakari, *Practical MEMS* (Small Gear Publishing, Las Vegas, NV, 2009).
[46]"1.6-GHz, low-noise, FET-input operational amplifier," Texas Instruments Datasheet No. OPA657, 2015.
[47]H. Nyquist, Phys. Rev. **32**, 110 (1928).
[48]P. R. Saulson, Phys. Rev. D **42**, 2437 (1990).

© Author(s) 2020